Density Functional Theory of the Water Splitting Reaction on Fe(0): Comparison of Local and Nonlocal Correlation Functionals

Junwei Lucas Bao, Haoyu S. Yu, Kaining Duanmu, Maxim A. Makeev, Xuefei Xu, and Donald G. Truhlar*

Department of Chemistry, Chemical Theory Center, Inorganometallic Catalyst Design Center, and Supercomputing Institute, University of Minnesota, 207 Pleasant Street SE, Minneapolis, Minnesota 55455-0431, United States

S *Supporting Information*

ABSTRACT: Metal clusters have broad applicability in catalysis due to their unique reactivity and chemical selectivity, and density functional theory has become an important method for understanding catalysis and attempting to design better catalysts. In the present paper, a main focus is on the correlation part of the exchange-correlation functional, and we tested the reliability of the Kohn−Sham density functional theory with local correlation functionals and with the nonlocal random phase approximation (RPA) correlation functional for the water splitting reaction on monatomic Fe(0) and, by implication, for transition-metal-catalyzed reactions more generally. We computed four barrier heights and six energies of reaction in the catalytic mechanism. If the results are judged by deviation from CCSD(T) calculations, it is found that many modern exchange-correlation (xc) functionals (about half of the functionals tested) with local correlation perform better than those using RPA nonlocal correlation; for example, the PWB6K, B97-3, ωB97X-D, MPW1K, M06-2X, and M05-2X hybrid xc functionals with local correlation have overall mean unsigned deviations of 1.9 kcal/mol or less from the CCSD(T) results, in comparison to a mean unsigned deviation of 3.5 kcal/mol for EXX-RPA@PBE. We also find significant differences between the predictions for catalysis at the Fe(100) surface. This work provides guidance and challenges for future theoretical investigations of transition-metal catalysis.

KEYWORDS: catalysis, density functional theory, electron correlation, exchange-correlation functionals, random phase approximation, transition metal, water splitting
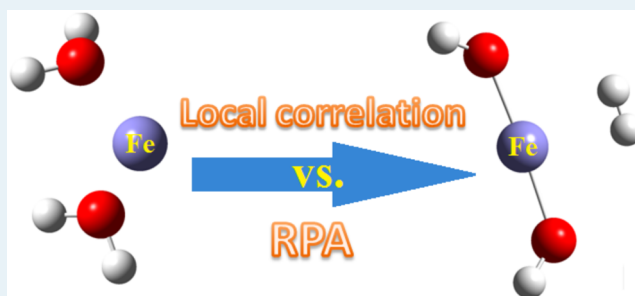
1. INTRODUCTION

Kohn−Sham density functional theory[1,2] (DFT) has been an indispensible tool in modern catalytic, organometallic, and functional materials research due to its excellent performance-to-cost ratio. With the exact exchange-correlation (xc) functional in hand, the method would provide an exact treatment of all the complicated many-body electronic interactions while retaining the computational simplicity of an independent-particle method such as the Hartree−Fock approximation. However, the accurate functional form of the exchange-correlation energy remains an enigma. Therefore, approximations of the xc functionals have to be made in order to provide practical predictions via DFT calculations. Some xc functionals have a set of parameters which are fitted over selected training sets (including experimental and/or high-level wave function data) with functional forms incorporating some predefined constraints, others are based on an empirical choice of constraints and functional forms, and variations on these themes are also possible—a variety of approaches to approximating the xc functional are available. Essentially all the xc functionals possess some empirical and ad hoc ingredients, and their accuracy for practical problems can only be ascertained by testing them against reliable experimental data or reliable theoretical data, with the latter only available for a limited number of very small systems.

Metal clusters and single-metal-atom clusters[3−15] have played an increasingly important role in catalytic chemistry due to their high selectivity and chemical reactivity combined with experimental advances in the preparation of well-characterized, size-selected metal clusters. For instance, it has been shown that an encapsulated copper cluster can be a catalyst for hydrogenation with renewability and high chemoselectivity.[14] Electronic structure computations, such as DFT, or wave function methods, such as coupled cluster theory and multireference calculations, can contribute significantly to our understanding of the mechanisms of metal-cluster catalysis at the molecular level, and they can eventually lead us to the next generation of catalysts. However, reliable wave function methods remain impractically expensive for all but the simplest systems, and, because of the multireference open-shell character of catalysts containing transition metals, it is a very challenging task to develop computationally efficient xc functionals that can make reliable predictions. The first step toward achieving this

goal is to ascertain the accuracy of existing xc functionals for systems small enough to obtain reliable benchmark results by wave function theory, for example, small metal clusters or monatomic metallic systems of the first-row transition metals, such as iron, cobalt, nickel, and copper, and to learn from both the successes and the failures.

Exchange-correlation functionals may be local (by which we mean that they depend only on local variables such as the local spin densities, their gradients, and the spin-resolved local kinetic energy densities) or nonlocal, where the latter, until recently, has usually meant that nonlocal Hartree–Fock exchange is included. One motivation for including nonlocal Hartree–Fock exchange is that the original local xc functionals such as PW91[16] significantly and systematically underestimate barrier heights and overestimate bond energies,[17,18] although these problems have been ameliorated and to some extent have been overcome with modern local functionals.[19–21] More recently some workers have begun to include nonlocal correlation.[22–29] (Functionals with nonlocal exchange are often called hybrid, and functionals that also have nonlocal correlation have been called doubly hybrid.) Recently Karlický and co-workers[30] studied the water-splitting reaction on zerovalent iron with a few local-correlation xc functionals with both local and nonlocal approximations to exchange and compared the results to non-self-consistent random phase approximation (RPA) calculations that involved two steps: first a calculation with the local PBE[31] exchange-correlation functional to get orbitals and then a post-SCF calculation employing these orbitals with nonlocal Hartree–Fock exchange and nonlocal random phase approximation[23,24,28,29,32–34] (RPA) correlation. The latter calculation has been labeled EXX-RPA,[35] and the combination with the first step has been called EXX-RPA@PBE; we will follow that naming convention here. Karlický and co-workers judged the density functional theories by comparison of their results to values obtained by coupled cluster wave function theory and concluded that EXX-RPA@PBE provides a systematic improvement over methods with local correlation and therefore should serve as an accurate and efficient (in comparison with coupled cluster calculations) method in metallic catalytic studies and surface chemistry.

The theoretical foundations of the EXX-RPA method and applications to various material systems have recently been reviewed, and the reader is directed to those reviews for background.[36,37] Karlický and co-workers concluded that the RPA "provides a physically correct description of adsorption and systematically improved reaction barriers" in comparison to local functionals, whose performance was gauged by the PW91 local xc functional, and even in comparison to hybrid functionals that have nonlocal exchange. This conclusion could give the impression that using RPA nonlocal correlation is inherently more accurate or more accurate at the current state of development than using DFT with local correlation functionals. If true, this would be an important conclusion because DFT with nonlocal functionals is more expensive than DFT with local functionals, especially for extended systems. One goal of the present work is to test whether this conclusion is justified. We therefore compare the results of DFT calculations with RPA correlation against DFT calculations with local correlation and against DFT calculations with both exchange and correlation being local. Following the criterion for accuracy chosen in the work of Karlický and co-workers, we base our judgments on deviations from coupled cluster calculations; the details of the coupled cluster calculations are

given in section 3.2, and the validity using coupled cluster data as reference data is tested and discussed in section 3.1. Such tests for gas-phase catalysis are reported in section 3.3. Our tests include the Minnesota functionals, which have shown excellent performances for a variety of chemically important systems,[38–40] and we also compare results to several other frequently used xc functionals with local correlation to test whether RPA provides higher accuracy than existing functionals with local correlation. Section 3.4 presents results for catalysis at a solid–vacuum interface, for which there are no reference data at the present time, however.

Previous work[41] has reported calculations for the reaction Fe + H_2O → FeO + H_2. The first step of this reaction, i.e., Fe + H_2O → HFeOH, is the same as that for the reaction we consider in this work. The role of the diffuse functions has been reported for the first step of the reaction we consider in the current work,[41] but the previous coupled cluster calculations[30] for the following steps in the presently studied reaction did not include diffuse functions, whose effect is tested here.

Filip and co-workers have carried out experimental work using Fe Mössbauer spectroscopy and computational work to investigate the mechanism and kinetics of the Fe(0) nanoparticle–water reactions.[42] Theoretical modeling of zerovalent iron nanoparticles is of great importance for their increasingly practical applications, and predicting their nanoscale chemistry via computational tools with a high performance-to-cost ratio is very challenging.[43] Eder et al. carried out periodic density functional calculations to study the initial stage of the iron(100) and iron(110) surface–water oxidation reaction, which involves the dissociation of the water molecule;[44] the dissociation of water on an iron surface has also been investigated using GGA functionals and range-separated hybrid functionals.[45]

The water-splitting reaction on Fe(0), which results in the production of molecular hydrogen, has five elementary steps as summarized in Table 1; these processes involve both transition-metal reaction chemistry and physisorption, and hence they provide a broad testing ground.

Table 1. Mechanism of the Water Splitting Reaction on Fe(0)

step	description	reaction
R1	formation of first vdW complex	Fe + H_2O → Fe···OH_2
R2	hydrogen migration reaction	Fe···OH_2 → HFeOH
R3	formation of second vdW complex	HFeOH + H_2O → HFeOH···H_2O
R4	dehydrogenation	HFeOH···H_2O → HOFeOH···H_2
R5	dissociation of third vdW complex	HOFeOH···H_2 → HOFeOH + H_2
net (R_O)	water splitting on Fe(0)	Fe + $2H_2O$ → HOFeOH + H_2

We computed the classical (zero-point-energy exclusive) barrier heights and classical energies of reaction for all these reactions, and all our comparisons of theoretical results are made on a consistent basis of including electronic energies and nuclear repulsion but not vibration.

2. COMPUTATIONAL DETAILS

In the present study, a relatively broad range of density functionals has been employed to compute the barrier heights and energies of reaction for the five-step zerovalent atomic iron–water reaction. We classified the density functionals tested in the current work into five groups, as delineated in Table 2. As indicated in this table, the readers could refer

Table 2. Density Functionals Tested in the Current Work

type	exchange	correlation	standard name
generalized gradient approximation (GGA)	local	local	BLYP[50]
			MOHLYP[51]
			MPWLYP1W[52]
			PBE[31]
			PBEsol[53]
			PBE1W[52]
			PBELYP1W[52]
			SOGGA[54]
			SOGGA11[55]
nonseparable gradient approximation (NGA)	local	local	N12[56]
meta-GGA	local	local	M06-L[19]
			revTPSS[57]
			TPSSLYP1W[52]
			τ-HCTH[58]
range-separated meta-GGA	local	local	M11-L[20]
meta-NGA	local	local	MN12-L[21]
global-hybrid GGA	nonlocal	local	B3LYP[59]
			B97−1[60]
			B97−2[61]
			B97−3[62]
			MPW1K[63]
			PBE0[64]
			SOGGA11-X[65]
global-hybrid meta-GGA	nonlocal	local	M05[66]
			M05-2X[67]
			M06[68]
			M06-2X[68]
			M06-HF[69]
			M08-HX[70]
			M08-SO[70]
			PW6B95[71]
			PWB6K[71]
range-separated hybrid GGA	nonlocal	local	ωB97X[72]
range-separated hybrid meta-GGA	nonlocal	local	M11[73]
screened-exchange hybrid GGA	nonlocal	local	HSE06[74]
screened-exchange hybrid NGA	nonlocal	local	N12-SX[75]
screened-exchange hybrid meta-NGA	nonlocal	local	MN12-SX[75]
meta-GGA +MM[a]	nonlocal	local	M06-L-D3[19,76]
global-hybrid meta-GGA + MM[a]	nonlocal	local	PW6B95-D3(BJ)[71,77]
range-separated hybrid GGA +MM[a]	nonlocal	local	ωB97X-D[78]
exact exchange + nonlocal correlation	nonlocal	nonlocal	EXX-RPA@PBE[31−34]

[a]+MM denotes the addition of a molecular mechanics damped dispersion term.

to references 19−21, 31−34, and 42−70 for further details of the density functionals we tested in the current work. We note that functionals labeled as "range-separated hybrid ...", "range-separated meta-GGA", and "screened-exchange" are all range-separated, but in different ways. Range-separated hybrids have a percentage (called X) of Hartree−Fock exchange that increases as a function of internuclear distance (called r_{12}), screened-exchange functions have an X value that decreases to 0 at large, and a range-separated meta-GGA is local for both small and large r_{12}, although it has a different local form in the two ranges.

In order to perform a consistent comparison, all these density functional calculations on atoms and molecules have been carried out with the cc-pVQZ[46,47] basis at the geometries optimized by B97-1/cc-pVTZ.[46,47] These geometries are adopted from the previous work[30] for a consistent comparison. In all density functional calculations on atomic and molecular systems, stability tests[48,49] of the Slater determinant have been carried out in order to find the most stable broken-symmetry solution.

The treatment of transition-metal systems is sometimes troubled by spin contamination of the Kohn−Sham determinant due to the intrinsically multidimensional character of the wave function and static correlation effects. Although one could anticipate that the systems studied here are high-spin systems with little spin contamination, we double-checked this as follows. The M06-L xc functional has been found to be able to predict correct spin multiplicity for a variety of transition-metal systems,[79] and we used this functional to find the lowest spin state for the systems considered here. In all species considered, Fe(0) is found to be in the high-spin state: i.e., the quintet state. The computed $\langle S^2 \rangle$ values by M06-L/cc-pVQZ//B97-1/cc-pVTZ level are 6.018, 6.023, 6.021, 6.019, 6.030, 6.022, 6.016, and 6.016 for Fe(0), Fe···H_2O, TS1, HFeOH, HFeOH···H_2O, TS2, Fe(OH)$_2$···H_2 and Fe(OH)$_2$, respectively. Because these values are close to the correct quintet value of 6.000, we conclude that spin contamination is not important in the reactions we investigated here.

Spin−orbit coupling is not negligible for many problems in transition-metal chemistry, especially for 4d and 5d elements, but sometimes also for 3d elements such as Fe. However, the main

Table 3. Relative Energies (in kcal/mol) of Various Species at the CCSD(T)-3s3p-DKH Level of Theory for the Fe(0)−H$_2$O System on the Basis of the B97-1/cc-pVTZ Geometries

basis set	Fe + 2H$_2$O	Fe−OH$_2$ + H$_2$O	TS1 + H$_2$O	HFeOH + H$_2$O	HFeOH − H$_2$O	TS2	Fe(OH)$_2$ − H$_2$	Fe(OH)$_2$ + H$_2$	MUD
TZ[a]	0.00	−3.72	27.46	−26.68	−43.34	−24.19	−47.52	−45.33	1.57
aTZ[b]	0.00	−2.57	27.41	−27.69	−43.14	−24.27	−49.14	−46.83	0.90
aQZ[c]	0.00	−2.78	27.01	−28.11	−43.78	−25.19	−49.81	−47.23	0.38
CBS(TZ, QZ)[d]	0.00	−2.90	26.90	−28.40	−44.20	−25.70	−50.20	−47.30	0.12
CBS(aTZ, aQZ)-1[e]	0.00	−2.93	26.64	−28.54	−44.43	−26.13	−50.49	−47.67	0.14
CBS(aTZ, aQZ)-2[f]	0.00	−2.90	26.61	−28.64	−44.55	−26.31	−50.63	−47.77	0.24
CBS(aTZ, aQZ)-3[g]	0.00	−2.84	26.77	−28.44	−44.26	−25.88	−50.32	−47.57	0.00
std deviation d−g	0.00	0.04	0.13	0.11	0.16	0.27	0.19	0.20	
std deviation e−g	0.00	0.05	0.09	0.10	0.15	0.22	0.16	0.10	

[a]cc-pwCVTZ-DK for Fe, cc-pVTZ for O, cc-pVTZ for H. [b]cc-pwCVTZ-DK for Fe, aug-cc-pVTZ for O, cc-pVTZ for H. [c]cc-pwCVQZ-DK for Fe, aug-cc-pVQZ for O, cc-pVQZ for H. [d]CBS limits extrapolated from TZ and QZ data points, as reported in ref 30. [e]CBS limits extrapolated from aTZ and aQZ data points using eq 4 with α = 3.4 and β = 2.4. [f]CBS limits extrapolated from aTZ and aQZ data points using eq 4 with α = 4.93 and β = 2.13. [g]CBS limits extrapolated from aTZ and aQZ data points using eqs 1−3.

quantitative comparisons in the present paper involve comparing density functional energies to coupled cluster calcuations and to one another, and the spin−orbit effects would largely cancel in such comparisons; thus, we did not include them in these comparisons. However, in the comparisons of coupled cluster and density functional theory calculations to experiment for diatomic molecules (discussed below), we do include spin−orbit effects for both atoms and molecules.

Reference values have been computed for the barrier heights and energies of reaction by coupled cluster theory with single and double excitations and a quasi-perturbative treatment of connected triple excitations[80] with the second-order Douglas−Kroll−Hess scalar relativistic method[81−84] and valence plus outer-core 3s3p electronic correlations, and with the two-point extrapolated complete basis set (CBS),[85−88] which we abbreviate as CCSD(T)-3s3p-DKH/CBS. As for the density functional calculations, all coupled cluster calculations are single-point energies at the geometries optimized by B97-1/cc-pVTZ. The reference values for the barrier heights and energies of reaction are obtained by extrapolating the aTZ and aQZ data points (see section 3.2 for details); these are the CBS-limit results in Table 3. In order to investigate the basis set effects in the coupled cluster calculations, triple-ζ (TZ), augmented-triple-ζ (aTZ), and augmented-quadruple-ζ (aQZ) basis sets are utilized: specifically, cc-pwCVTZ-DK for Fe,[47] cc-pVTZ for O,[46] and cc-pVTZ for H[46] in TZ calculations; cc-pwCVTZ-DK for Fe, aug-cc-pVTZ for O, and cc-pVTZ for H in aTZ calculations; cc-pwCVQZ-DK for Fe, aug-cc-pVQZ for O, and cc-pVQZ for H in aQZ calculations.

All of the electronic structure calculations on molecular and atomic systems were performed with a locally modified Gaussian 09[89] program, except that the data for FeH and FeCl in Table 4 were obtained with Molpro2010.1.[90]

The problem of a single water molecule on the (100) iron surface was treated using the Vienna ab initio simulation package (VASP).[91,92] The interactions between the valence electrons and core electron orbitals are described using the projector augmented wave (PAW) method,[93] as implemented by Kresse and Joubert.[94] The size of the basis set is determined by a cutoff energy, which was fixed at E_c = 400 eV throughout the calculations. In all the cases reported on here, spin-polarized atomic configurations (ISPIN = 2, in the keyword convention of VASP) are considered.

Three classes of exchange correlation functionals were tested for heterogeneous catalysis: (a) the M06-L and revTPSS meta-GGA functionals, (b) the HSE06 and N12-SX screened-exchange gradient approximations, and (c) EXX-RPA@PBE, defined above as the combination of Hartree−Fock exchange and RPA correlation in a post-SCF calculation with PBE orbitals. The EXX-RPA@PBE calculations were carried out using the adiabatic-connection fluctuation−dissipation theorem formulation of the RPA method, as implemented in the VASP code.[35] The methodology of calculations, adopted in this work, has previously been used to study CO

Table 4. Calculated Errors (kcal/mol) of CCSD(T)-3s3p-DKH/CBS Calculations for the Bond Dissociation Energies of FeH and FeCl in Comparison to Experimental Data

	error						
	aTZ[a]	aQZ[b]	CBS[c]	aTZ′[d]	aQZ′[e]	CBS′[f]	D_e (exptl)[g]
FeH[h]	2.1	4.6	6.3	2.1	4.6	6.3	36.9
FeCl[i]	−1.0	1.6	3.3	−1.2	1.3	2.9	78.5
MUE[j]	1.6	3.1	4.8	1.6	2.9	4.6	

[a]aTZ basis set: cc-pwCVTZ-DK for Fe, aug-cc-pVTZ for Cl, cc-pVTZ for H. [b]aQZ basis set: cc-pwCVQZ-DK for Fe, aug-cc-pVQZ for Cl, cc-pVQZ for H. [c]CBS(aTZ,aQZ)-3: CBS limits extrapolated from aTZ and aQZ data points by using eqs 1−3. [d]aTZ′ basis set: cc-pwCVTZ-DK for Fe, aug-cc-pVTZ-DK for Cl, cc-pVTZ-DK for H. [e]aQZ′ basis set: cc-pwCVQZ-DK for Fe, aug-cc-pVQZ-DK for Cl, cc-pVQZ-DK for H. [f]CBS′(aTZ′, aQZ′)-3: CBS limits extrapolated from aTZ′ and aQZ′ data points by using eqs 1−3. [g]Experimental data. [h]The bond lengths of FeH ($^4\Delta$) used in the calculations is 1.630 Å. [i]The bond length of FeCl ($^6\Delta$) used in the calculations is 2.179 Å. [j]MUE is the mean unsigned error of bond energies of the two molecules in comparison to experimental data.

adsorption on Cu(111)[95] and CO adsorption on Cu, 4d metals, and Pt.[28]

The six stationary points (four minima and two saddle points) were optimized using the PBE functional, and these geometries were used for the subsequent calculations with M06-L, revTPSS, HSE06, N12-SX, and EXX-RPA@PBE. All of the heterogeneous catalysis calculations use these PBE geometries, and PBE orbitals are used as the initial guess for the self-consistent-field cycles of both the meta-GGA and screened-exchange calculations.

The Fe(100) surface was described by a repeated slab, with the size in the direction perpendicular to the (100) surface being 3 times that in the lateral directions (the vacuum spacing thus being ~12.0 Å). The lateral dimensions of the slab correspond to p(3 × 3) surface structure (comprised of a total of 27 Fe atoms positioned in the calculation cell of parallelepiped-type geometry, stretched in the Z direction to accommodate the vacuum gap). The Brillouin zone integrations to obtain total energies were performed on Γ-centered grids of sizes 3 × 3 × 1 k points. The ionic relaxation was performed using the conjugate-gradient algorithm with the convergence criterion for the forces set to 10^{-4} eV/Å. The partial occupancies of orbitals were determined using the Methfessel−Paxton method,[96] which is known to perform well for metallic systems. The dissociation barriers were determined using the climbing image nudged elastic band method (CI-NEB),[97,98] as implemented[99] in the VASP program. For the M06-L calculations we used a very fine grid of 10 points/Å.

Table 5. Classical (Zero-Point-Energy Exclusive) Energies of Reaction ΔE_{rxn} for Reactions R1−R5 and the Overall Reaction R$_O$ and Forward and Reverse Classical Barrier Heights for Reactions R2 and R4[a]

xc functional	R1 ΔE_{rxn}	R2 V_f	R2 V_r	R2 ΔE_{rxn}	R3 ΔE_{rxn}	R4 V_f	R4 V_r	R4 ΔE_{rxn}	R5 ΔE_{rxn}	R$_O$ ΔE_{rxn}	barrier height MUD[b]	MSD[c]	TK MUD[d]
GGA and NGA Functionals													
MOHLYP	−6.06	19.80	43.38	−23.58	−8.72	11.60	21.77	−10.18	−2.61	−51.14	7.77	−7.77	5.65
PBELYP1W	−11.12	19.79	42.67	−22.89	−14.97	12.21	23.23	−11.02	1.49	−58.49	7.43	−7.43	5.87
BLYP	−10.24	18.75	42.45	−23.69	−13.94	11.70	22.58	−10.88	0.48	−58.28	8.04	−8.04	6.11
N12	−9.51	20.25	41.78	−21.53	−14.92	9.45	20.13	−10.68	0.93	−55.71	9.00	−9.00	6.22
MPWLYP1W	−11.39	19.06	42.38	−23.32	−15.16	11.77	21.55	−9.78	0.27	−59.38	8.22	−8.22	6.24
PBE1W	−11.58	17.81	41.76	−23.95	−15.21	11.01	20.70	−9.69	1.69	−58.73	9.09	−9.09	6.32
PW91[e]	−13.00	16.70	41.40	−24.70	−16.40	12.80	23.10	−10.30	3.80	−60.60	8.41	−8.41	6.36
PBE	−12.47	16.61	40.86	−24.25	−16.25	10.31	19.11	−8.81	2.22	−59.56	10.18	−10.18	6.74
SOGGA11	−8.93	18.60	41.16	−22.56	−11.13	7.46	16.43	−8.98	−1.30	−52.89	10.99	−10.99	7.01
PBEsol	−14.99	13.78	39.14	−25.36	−19.30	8.68	15.78	−7.10	3.62	−63.12	12.56	−12.56	8.36
SOGGA	−15.28	13.21	38.62	−25.41	−18.40	7.16	14.89	−7.72	3.74	−63.08	13.44	−13.44	8.71
Meta-GGA and Meta-NGA Functionals													
M11-L	−11.56	30.31	45.78	−15.47	−15.67	15.81	23.53	−7.71	1.01	−49.41	3.40	−3.05	3.78
M06-L	−11.39	23.70	50.24	−26.54	−19.05	16.53	21.72	−5.19	4.11	−58.06	3.86	−3.86	4.09
MN12-L	−14.10	31.33	44.16	−12.83	−16.96	18.38	23.39	−5.01	1.83	−47.05	3.46	−2.59	4.15
M06-L-D3	−11.38	23.33	49.88	−26.56	−19.08	16.52	21.72	−5.20	4.14	−58.07	4.04	−4.04	4.17
τHCTH	−10.17	18.83	45.36	−26.52	−15.89	10.71	19.72	−9.02	2.32	−59.29	8.25	−8.25	5.64
TPSSLYP1W	−11.24	18.48	46.41	−27.94	−14.95	12.22	26.95	−14.73	1.31	−67.54	7.15	−5.89	7.03
revTPSS	−12.00	15.03	46.83	−31.80	−15.95	11.79	25.09	−13.30	1.63	−71.43	7.55	−7.22	7.79
Hybrid GGA and Hybrid NGA Functionals													
B97-3	−5.19	29.30	53.46	−24.16	−13.77	16.26	22.56	−6.30	1.54	−47.88	1.51	−1.51	1.36
ωB97X-D	−7.33	29.16	55.18	−26.01	−16.24	17.03	22.74	−5.71	2.92	−52.37	0.88	−0.88	1.42
MPW1K	−4.64	28.23	56.15	−27.92	−15.42	17.85	21.37	−3.52	1.96	−49.54	1.48	−1.01	1.57
SOGGA11-X	−1.85	33.50	55.76	−22.26	−16.69	18.58	22.10	−3.52	3.15	−41.17	1.75	0.58	2.15
B97-2	−6.15	26.98	52.25	−25.28	−14.37	14.32	21.20	−6.88	1.81	−50.88	3.22	−3.22	2.30
ωB97X	−7.63	29.99	58.14	−28.16	−18.46	17.82	23.22	−5.40	4.48	−55.16	1.27	0.39	2.51
B97-1[e]	−7.60	26.60	51.20	−24.60	−16.00	14.40	21.20	−6.80	2.90	−52.10	3.56	−3.56	2.56
B3LYP	−8.81	25.52	49.75	−24.23	−14.55	15.17	22.85	−7.68	1.32	−53.95	3.58	−3.58	3.24
PBE0	−9.12	23.68	50.10	−26.42	−15.80	14.75	20.01	−5.26	2.32	−54.28	4.77	−4.77	3.42
HSE06[e]	−10.30	24.70	49.60	−24.90	−16.20	15.20	20.00	−4.80	2.10	−54.10	4.53	−4.53	3.51
N12-SX	−10.92	25.79	51.08	−25.29	−16.40	13.18	20.73	−7.55	2.52	−57.64	4.21	−4.21	3.76
Hybrid-Meta GGA and Hybrid Meta-NGA Functionals													
PWB6K	−4.12	31.63	57.45	−25.82	−17.11	18.75	22.85	−4.10	3.08	−48.07	1.56	0.77	1.18
M06-2X	−3.96	34.19	57.16	−22.97	−19.57	18.18	24.07	−5.89	4.89	−47.50	1.77	1.50	1.70
M05-2X	−1.33	34.87	60.41	−25.53	−18.86	17.22	23.32	−6.10	4.38	−47.45	3.18	2.05	1.91
M05	−4.55	31.60	52.26	−20.67	−17.98	16.71	22.76	−6.05	3.61	−45.63	2.07	−1.07	1.99
PW6B95	−7.95	26.66	51.47	−24.81	−16.04	15.95	22.71	−6.76	2.45	−53.12	2.71	−2.71	2.35
PW6B95-D3BJ	−8.48	26.79	51.45	−24.67	−16.62	15.93	22.65	−6.72	2.80	−53.69	2.70	−2.70	2.50
M08-HX	−4.73	33.50	61.21	−27.71	−19.03	19.22	22.24	−3.02	4.32	−50.17	3.23	2.14	2.74
M08-SO	−4.84	35.73	56.09	−20.35	−18.66	20.02	23.28	−3.26	4.07	−43.03	2.45	1.88	2.85
MN12-SX	−11.78	32.81	55.08	−22.28	−17.05	17.08	25.10	−8.02	2.64	−56.49	1.32	0.61	2.98
M06	−6.28	31.91	50.79	−18.88	−19.63	17.97	22.89	−4.93	5.59	−44.12	2.17	−1.02	3.00
M11	−8.60	22.07	61.52	−39.45	−18.04	18.74	21.94	−3.20	3.32	−65.96	4.18	−0.84	6.04
M06-HF	−26.06	36.32	61.78	−25.46	−19.92	18.56	24.40	−5.84	4.68	−72.61	3.38	3.36	6.81
Hartree−Fock Exchange + Nonlocal Correlation													
EXX-RPA@PBE[e]	−10.10	31.20	49.00	−17.80	−13.20	19.10	23.10	−4.00	−0.30	−45.40	2.47	−1.31	3.48
Benchmarks (Not Final)													
CCSD(T)/CBS(TZ, QZ)[e]	−2.90	29.80	55.30	−25.50	−15.80	18.50	24.50	−6.00	2.90	−47.30	0.12	0.12	0.11
CCSD(T)/ CBS(aTZ,aQZ)-1	−2.93	29.57	55.18	−25.61	−15.88	18.29	24.36	−6.06	2.83	−47.67	0.06	−0.06	0.06
CCSD(T)/CBS(aTZ, aQZ)-2	−2.90	29.51	55.25	−25.74	−15.91	18.24	24.32	−6.07	2.86	−47.77	0.09	−0.08	0.10
Final Reference Values													
CCSD(T)/CBS(aTZ, aQZ)-3	−2.84	29.61	55.21	−25.59	−15.82	18.37	24.43	−6.06	2.75	−47.57	0.00	0.00	0.00

[a]The unit is kcal/mol; single-point energy calculations of various density functionals with the cc-pVQZ basis are performed using B97-1/cc-pVTZ geometries with ultrafine integral grids; mean unsigned deviations (MUDs) and mean signed deviations (MSDs) are computed with respect to

Table 5. continued

CCSD(T)-3s3p-DKH/CBS results, which are the final reference values labeled as "CCSD(T)/CBS(aTZ,aQZ)-3" in the table. [b]Mean unsigned deviations (MUDs) for the four barrier heights. [c]Mean signed deviations (MSDs) for the four barrier heights. [d]MUDs for full thermochemical kinetics (TK): i.e., both energies of reaction and forward and reverse barrier heights of all reactions. [e]Computed from the data reported in ref 30.

3. RESULTS AND DISCUSSION

3.1. Utility of Coupled Cluster Calculations To Serve as Reference Data.
A recent test[100] against experimental bond energies for 20 diatomic molecules that contain a 3d transition metal and that have estimated experimental errors of 2 kcal/mol or less showed that—on average—CCSD(T) with a minimally augmented multiply polarized triple-ζ basis set has errors comparable to, but not smaller than, the errors of the best Kohn–Sham density functionals. Two of the 20 diatomics, in particular FeH and FeCl, contain an iron atom, and in Table 4 (Table 4 gives the calculated errors (kcal/mol) at the CCSD(T)-3s3p-DKH/CBS level for bond dissociation energies of FeH and FeCl in comparison to the experimental data), we present tests for these two molecules showing that increasing the basis set toward the complete-basis-set (CBS) limit does not systematically remove the discrepancy of CCSD(T) from experiment. It was concluded[100] on the basis of the results for the 20 diatomics that CCSD(T) cannot *in general* serve as a benchmark for testing Kohn–Sham density functional theory, and these additional basis set tests do not change that conclusion.

The 20 diatomic molecules in the previous study comprise a diverse set of molecules, but in the present study the only transition metal element is iron. We therefore analyzed the previous study from another point of view, considering results from 41 exchange-correlation functions plus the MP2 and CCSD methods. For each diatomic molecule, we ranked these 43 approximate methods based on the magnitude of the deviation from CCSD(T)-3s3p-DKH/apTZ calculations (apTZ denotes aug-cc-pwCVTZ-DK basis sets for transition-metal elements and aug-cc-pVTZ-DK basis sets for other elements), and we also ranked them in terms of the magnitude of their deviation from experiment. We then did a Spearman rank correlation analysis of the two ranks. For some molecules, the correlation is good (as high as 0.992), and for others it is very bad (the lowest being −0.62, the average being 0.75). However, for FeH the Spearman correlation coefficient is 0.989, and for FeCl it is 0.982. Therefore, since both of these values are reasonably high, and although we should be cautious not to overinterpret the results, we conclude that we can tentatively use the CCSD(T)/CBS results in the present paper as reference values for judging the relative accuracy of other methods for the Fe-atom mechanism.

3.2. Basis Set Effects in CCSD(T) Calculations.
The present section has two purposes: (1) to test the effect of diffuse basis functions on the reference results and (2) to test the effect of different methods of extrapolation to the complete basis set (CBS) limit.

Table 3 shows the computed relative energies of all the species involved in the iron−water reaction at the CCSD(T)-3s3p-DKH level. The rows labeled CBS are obtained by separately extrapolating the Hartree−Fock and correlation energies to the complete basis set limit. The last column shows the mean unsigned deviation (MUD) relative to the most complete calculation, which is called the final reference value. For the final reference values, the CBS limits are based on the equations[101]

$$E_{CBS}^{corr} = \frac{X^3 E_X^{corr} - (X-1)^3 E_{X-1}^{corr}}{X^3 - (X-1)^3} \tag{1}$$

$$E_{CBS}^{HF} = \frac{E_{X-1}^{HF} - \lambda E_X^{HF}}{1 - \lambda} \tag{2}$$

where

$$\lambda = \frac{X}{X+1} \exp[9(\sqrt{X} - \sqrt{X-1})] \tag{3}$$

In the above equations, X and $X - 1$ represent a pair of basis sets with successive cardinalities, which are aQZ ($X = 4$) and aTZ ($X - 1 = 3$) respectively in our study; "corr" stands for correlation energies, and "HF" represents Hartree−Fock energies. Equation 3 is derived from the Karton−Martin two-point formula,[87] which has also been employed in the extrapolation of CCSD(T) results to the CBS limits.[101] The final extrapolated CCSD(T) energy, denoted as CBS-(aTZ,aQZ)-3, is computed as the summation of the correlation energy and the Hartree−Fock energy.

For comparison, we also carried out two other extrapolations, which were performed with the equation[86]

$$E_{CBS}^{CCSD(T)} = \frac{X^\alpha E_X^{HF} - (X-1)^\alpha E_{X-1}^{HF}}{X^\alpha - (X-1)^\alpha}$$
$$+ \frac{X^\beta E_X^{corr} - (X-1)^\beta E_{X-1}^{corr}}{X^\beta - (X-1)^\beta} \tag{4}$$

The CBS limits obtained with aTZ and aQZ data points using parameters $\alpha = 3.4$ and $\beta = 2.4$ are denoted by CBS(aTZ,aQZ)-1. These two parameters are fitted for extrapolating DZ and TZ to CBS limits.[86] Another set of parameters, $\alpha = 4.93$ and $\beta = 2.13$, which are fitted for extrapolating aDZ and aTZ to CBS limits,[102] can also be used to extrapolate aTZ and aQZ data points. The obtained CBS limits are denoted by CBS(aTZ,aQZ)-2. The CBS limits extrapolated from TZ and QZ data points, denoted by CBS(TZ,QZ), as reported in ref 30 are also included in Table 5.

The mean unsigned deviation of CBS(TZ,QZ) is 0.12 kcal/mol, which is insignificant in comparison to the relative energy of each species. Therefore, adding diffuse functions on oxygen atoms does not have a noticeable impact on the CCSD(T) results for this system. The CBS limits from the four different approaches are very close to each other; the standard deviations of these four extrapolated methods for the relative energies of all the species are all smaller than 0.30 kcal/mol.

3.3. Barrier Heights and Energies of Reaction by Density Functional Theory for Catalysis at the Bare Metal Atom.
Figure 1 shows the schematic energy profile of all the steps involved in the water-splitting reaction on Fe(0).

Table 5 gives the classical (zero-point-energy exclusive) forward and reverse barrier heights for reactions R2 and R4 (four barrier heights) and the classical energies of reaction for R1−R5 and the overall reaction R_O (six reaction energies). The mean unsigned deviations (MUDs) and mean signed deviations (MSDs) are computed with respect to the final reference value
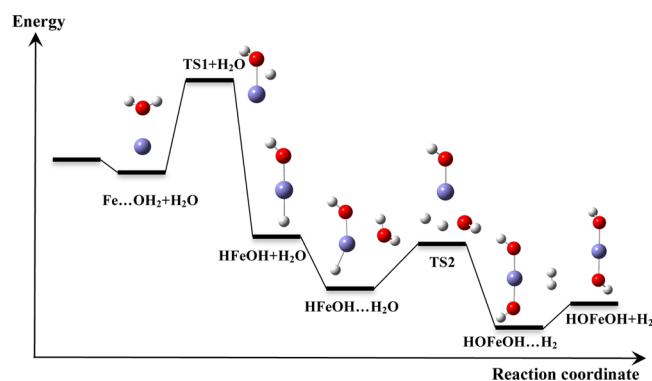
Figure 1. Schematic energy profile of the five-step water-splitting reaction at atomic Fe(0).

explained above. In each group of xc functionals in Table 5, the functionals are ordered with respect to their overall MUDs for the 10 data; these MUDs are labeled TK for "thermochemical kinetics". Table 6 shows the percentage of Hartree–Fock exchange in the hybrid functionals we tested in the present work.

As we can see from the last column of Table 5, the overall MUDs depend strongly on the ingredients of the xc functional, being 5.6–8.7 kcal/mol for GGAs, 6.2 kcal/mol for the NGA, 3.8–7.8 kcal/mol for meta-GGAs, 4.15 kcal/mol for the meta-NGA, 3.5 for the functional with nonlocal correlation, and 1.2–6.8 kcal/mol for hybrid functionals. However, most hybrid functionals yield errors closer to the lower end than the higher end of that range, with 21 of 23 hybrid functionals having MUDs in the range 1.2–3.8 and the other two having MUDs of 6.0 and 6.8 kcal/mol. Table 6 shows that the two hybrid functionals with the largest overall MUDs are among those with the highest percentages of Hartree–Fock exchange.

The EXX-RPA@PBE calculations have an overall MUD lower than those for all 18 local functionals, but their overall MUD is lower than only 2 of the 23 hybrid functionals, which have nonlocal exchange.

If we consider the mean unsigned deviations of the four barriers, eight of the density functionals developed by us, namely MPW1K, SOGGA11-X, MN12-SX, M05, M06, M06-2X, M08-SO, and PWB6K, provide—on average—more accurate predictions than EXX-RPA@PBE, and three density functionals developed elsewhere (B97-3, ωB97X-D, ωB97X) also do so. If we consider the overall performances for both the barrier heights and the energies of reaction, 11 density

functionals developed in our group (MPW1K, SOGGA11-X, MN12-SX, M05, M05-2X, M06, M06-2X, M08-HX, M08-SO, PWB6K, and PW6B95) and 8 density functionals developed elsewhere (B97-3, ωB97X-D, B97-2, ωB97X, B97-1, B3LYP, PBE0, and PW6B95-D3(BJ)) have smaller overall mean unsigned deviations than the nonlocal-correlation method EXX-RPA@PBE.

Among all of these tested functionals, five have mean unsigned deviations in the range 1.2–1.7 kcal/mol. This is an encouraging result for this very challenging transition-metal system, which not only involves the multireference character but also involves physisorption that is sensitive to noncovalent interactions.

The averaged overall MUD of the GGA/NGA, meta-GGA/meta-NGA, hybrid GGA/hybrid NGA, hybrid meta-GGA/hybrid meta-NGA, and RPA functionals examined in the current work are respectively 6.7, 5.2, 2.5, 3.0, and 3.5 kcal/mol. Therefore, the hybrid functionals give the best predictions for this system. From the MSD values given in Table 5, we found that most of the density functional methods underestimate the barrier heights. The averaged MSD for the GGA, meta-GGA, hybrid GGA, and hybrid meta-GGA functionals are respectively −9.56, −4.99, −2.39, and 0.33 kcal/mol. Therefore, the hybrid meta-GGA functionals provide the best prediction for the barrier heights for this system. RPA gives an overall MUD of 3.48 kcal/mol and has an error of 7.26 kcal/mol for the energy of reaction of R1.

PWB6K gave the smallest overall mean unsigned deviation from CCSD(T) for this system; ωB97X-D gave the smallest mean unsigned deviation for all of the reaction barrier heights.

Another way to put the present findings into perspective is to note that Scuseria and co-workers[103] showed that the RPA is identical to an approximation to coupled cluster theory with only double excitations (CCD) in which only the ring diagrams are retained (ring-CCD). In this context it is notable that even full coupled cluster theory with both single and double excitations (CCSD without the approximation of being restricted to ring diagrams) has been shown to be less accurate than many local-correlation exchange-correlation density functionals for barrier heights.[104] For the most complete basis set tested in each case, the mean unsigned error on 24 diverse barrier heights (for reactions involving only nonmetal elements) was found to be 0.5 kcal/mol for CCSD(T), 2.2 kcal/mol for CCSD, and 0.9 kcal/mol for M06-2X.[104] However, as a possible path to future improvement, we note that CCSD is well suited to the introduction of semiempirical

Table 6. Hybrid Functionals Tested in the Current Work and Their Percentage of Nonlocal Hartree−Fock Exchange (% X)

density functional	% X	density functional	% X	density functional	% X
ωB97X	15.77–100[a]	PBE0	25	PWB6K	46
B3LYP	20	B97-3	26.93	M08-HX	52.23
B97-1	21	M06	27	M06-2X	54
B97-2	21	M05	28	M05-2X	56
ωB97X-D	22.2–100[a]	PW6B95	28	M08-SO	56.79
HSE06	25–0[b]	SOGGA11-X	35.42	EXX-RPA@PBE	100@0[c]
N12-SX	25–0[b]	MPW1K	42.8	M06-HF	100
MN12-SX	25–0[b]	M11	42.8–100[a]		

[a]The percentage of Hartree−Fock exchange increases from the first value listed for small interelectronic separation to 100% at large interelectronic separation. [b]The percentage of Hartree−Fock exchange decreases from 25% at small interelectronic separation to 0 at large interelectronic separation. [c]The percentage of Hartree−Fock exchange is 100% in the post-SCF calculation on the basis of orbitals obtained with no Hartree−Fock exchange.
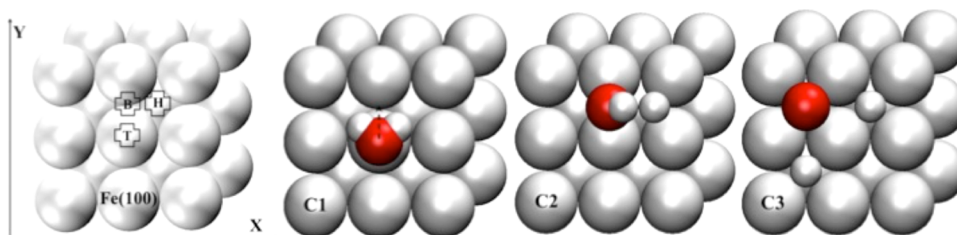
Figure 2. Illustration of the Fe + H₂O → H−Fe−O−H reaction on the iron(100) surface. The first snapshot illustrates the Fe(100) slab surface used in the calculation and provides a definition of the three adsorption sites on the surface: (1) top (T), (2) bridge (B), and (3) hollow (H). C1 is a graphical illustration of the initial configuration, corresponding to the locally stable site on the surface (T). The process of dissociation proceeds by a water molecule moving toward the bridge site (B). At this site the molecule rotates in the $(z−x)$ plane with concurrent elongation of one of the O−H bonds, such that it breaks. The free hydrogen atom moves to the hollow (H) site, while the O−H moiety remains at the B location. In the final stage of dissociation (C3), the corresponding three atoms are distributed on the hollow sites.

improvements, and the mean unsigned error on the same data set for the BMC-CCSD method,[105] which is based on CCSD with five empirical parameters, reduced the error on the same data set (which was not used in its parametrization) to 0.7 kcal/mol. The QCISD ("quadratic configuration interaction with single and double excitations") method, which consists of a subset of the terms in CCSD (but a subset different from those used in ring-CCD), has also been incorporated in a double hybrid density functional (with five empirical parameters) that reduced the error on a different barrier height database to 0.6 kcal/mol (in comparison to 2.8 kcal/mol for straight QCISD).[106]

3.4. Barrier Heights and Energies of Reaction by Density Functional Theory for Catalysis at the Solid−Vacuum Interface. In the preceding section, it was shown that several density functionals provide an adequate description of the water dissociation on Fe(0) reactions in the gas phase, and a variety of local-correlation functionals correlate better with CCSD(T) than does EXX-RPA@PBE. However, the question as to what extent these conclusions are applicable to the problem of chemical reactions on metal surfaces remains to be addressed.

Chemical reactions on metal surfaces are sufficiently different from those in the gas phase that it is imperative to assess the influence of extended metal surfaces on the mechanisms and energetics of chemical reactions and on the validity of various theoretical approaches that may be applied to them.

Here we compare the predictions of several methods of describing adsorption and dissociation of a water molecule on the iron (100) surface. Two kinds of structures are considered, namely four equilibrium adsorption structures and two transition structures, where the latter are first-order saddle points. The relative energies for the structures were computed by

$$\Delta E_{structure} = E_{FeH_2O} - (E_{slab} + E_{H_2O}) \qquad (5)$$

where E_{FeH_2O} is the total energy of the structure on the metal surface, E_{slab} is the energy of the bare iron slab, and E_{H_2O} is the energy of a gas-phase water molecule.

Figure 2 illustrates the water dissociation reaction mechanism on the Fe(100) surface. Following ref 30 and a reference therein, we optimized six stationary points: four minima labeled C0−C3 and two saddle points labeled B1 and B2. The first stationary point, C0, corresponds to the bare surface with a water molecule infinitely separated. The second, C1, is the physisorbed water flat on the surface, with the oxygen atom over an iron atom, i.e., at an on-top site labeled T in Figure 2.

Water dissociation at 250 K results in formation of a p(1 × 2)−OH monolayer on the surface, with O−H bonds being tilted with respect to the surface normal. Correspondingly, the third minimum-energy structure, C2, corresponds to OH located at the bridge site (B) and H chemisorbed on an adjacent hollow site (H). The fourth minimum-energy structure, C3, corresponds to the OH moiety also having dissociated with all three atoms now at separate hollow sites. The saddle point B1 connects C1 to C2, and saddle point B2 connects C2 to C3. The trends of the energetics of these steps are summarized in Figure 3, where the relative energies defined by eq 5 are presented.
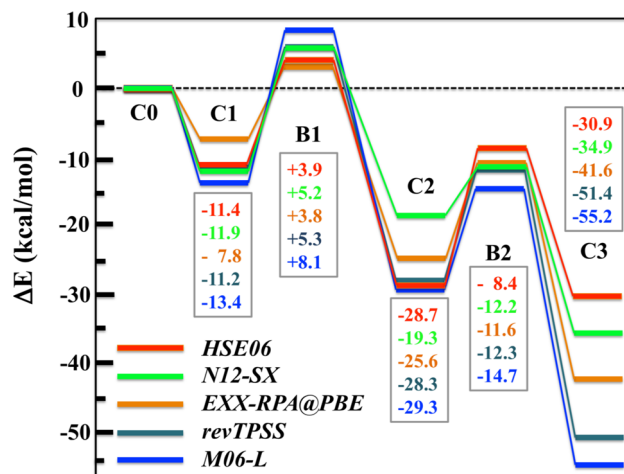

Figure 3. Relative energies for equilibrium structures C1−C3 (see Figure 2) and transition structures B1 and B2, as calculated by five density functional methods at geometries optimized by PBE. All energies are given in kcal/mol.

First we note that our EXX-RPA@PBE calculations give results similar to those of Karlický et al.[30] but show some quantitative differences that may be due to a different sample relaxation methodology and slab size used in our calculations (see above), as well as to different density functionals used to optimize geometries. Similarly our HSE06 calculations are quantitatively similar to those reported in ref 30, showing that the present use of PBE geometries leads to only minor differences from their calcuations with PW91 geometries.

One interesting trend in Figure 3, where all results are for the same size slab, is that, as functions of the reaction coordinate, the two screened-exchange functionals HSE06 and N12-SX give flatter potentials than does EXX-RPA@PBE, and the two

meta functionals M06-L and revTPS give more widely varying potentials. A set of five energies, as in Figure 3, has 15 pairs of energies (1−2, 1−3, 1−4, 1−5, 2−3, etc.), and we can compare various pairs of functionals with one another by computing the average difference in these 15 relative energies. Doing this shows that revTPSS and N12-SX both agree with EXX-RPA@PBE within 4−5 kcal/mol, on average, while M06-L and HSE06 differ from EXX-RPA@PBE by 6 kcal/mol, on average.

Further studies are needed to understand which of the five sets of results in Figure 3 is the most accurate, but since HSE06, N12-SX, and M06-L have only slightly larger deviations than EXX-RPA@PBE from CCSD(T) results for the single-atom catalytic mechanism, where CCSD(T) results are available, it is quite possible that these less expensive and simple calculations can be a fair alternative to the RPA approach. Further understanding will require a direct comparison to quantitatively accurate experimental or theoretical results, neither of which is available for the heterogeneous catalysis case.

4. CONCLUSION

In the current work, we first re-examined the reference CCSD(T) results for the water splitting reaction on a zerovalent iron atom. We found that adding diffuse basis functions on oxygen does not have a noticeable effect on the coupled cluster results for all of the reaction steps involved, which is consistent with the conclusion obtained previously[41] for the first step of the reaction.

Then, continuing with the zerovalent atomic iron catalyst for the water-splitting reaction, 41 density functionals with local correlation and 1 (EXX-RPA@PBE) with nonlocal correlation were tested against the reference results for 6 reaction energies and 4 barrier heights involved in the mechanism. We found that 19 of the functionals with local correlation had smaller average absolute errors than the functional with nonlocal correlation. This indicates that previous conclusions[30] that there is a systematic improvement in the accuracy of density functional theory from the generalized gradient approximation, to hybrid functionals, to the random phase approximation, are incorrect. On the basis of our investigation, the hybrid GGA functionals give the best overall mean unsigned deviation from the reference values for barrier heights and reaction energies combined, whereas hybrid meta-GGA functionals offer the best prediction if one only considers barrier heights. Most of the density functionals, including RPA, underestimate the barrier heights of this system. Only a few functionals, namely ωB97X, SOGGA11-X, MN12-SX, and PWB6K, give a mean unsigned deviation for barriers that is smaller than 1.0 kcal/mol.

Finally, we have presented a smaller study of the water splitting reaction on the (100) surface of iron. However, the lack of enough solid experimental data or benchmark wave function data on the mechanism of water dissociation and, particularly, barrier heights prevent quantitative evaluation of the performance for this heterogeneous case. This presents a challenge for future work.

ASSOCIATED CONTENT

Ⓢ Supporting Information

The following file is available free of charge on the ACS Publications website at DOI: 10.1021/cs501675t.

> Optimized geometries and absolute energies of all the structures in hartrees (PDF)

■ AUTHOR INFORMATION

Corresponding Author

*E-mail for D.G.T.: truhlar@umn.edu.

Notes

The authors declare no competing financial interest.

■ REFERENCES

(1) Hohenberg, P.; Kohn, W. *Phys. Rev.* **1964**, *136*, B864−B871.
(2) Kohn, W.; Sham, L. J. *Phys. Rev.* **1965**, *140*, A1133−A1138.
(3) Uzun, A.; Ortalan, V.; Browning, N. D.; Gates, B. C. *Chem. Commun.* **2009**, *31*, 4657−4659.
(4) Shimizu, K.; Ohshima, K.; Satsuma, A. *Chem. Eur. J.* **2009**, *15*, 9977−9980.
(5) Johnson, G. E.; Mitrić, R.; Bonačić-Koutecký, V.; Castleman, A. W., Jr. *Chem. Phys. Lett.* **2009**, *475*, 1−9.
(6) Lopez-Acevedo, O.; Kacprzak, K. A.; Akola, J.; Häkkinen, H. *Nat. Chem.* **2010**, *2*, 329−334.
(7) Yardimci, D.; Serna, P.; Gates, B. C. *ACS Catal.* **2012**, *2*, 2100−2113.
(8) Aydin, C.; Lu, J.; Browning, N. D.; Gates, B. C. *Angew. Chem., Int. Ed.* **2012**, *51*, 5929−5934.
(9) Flytzani-Stephanopoulos, M.; Gates, B. C. *Annu. Rev. Chem. Biomol. Eng.* **2012**, *3*, 545−574.
(10) An, K.; Somorjai, G. A. *ChemCatChem* **2012**, *4*, 1512−1524.
(11) Lu, Y.; Chen, W. *Chem. Soc. Rev.* **2012**, *41*, 3594−3623.
(12) Dhakshinamoorthy, A.; Garcia, H. *Chem. Soc. Rev.* **2012**, *41*, 5262−5284.
(13) Dal Santo, V.; Guidotti, M.; Psaro, R.; Marchese, L.; Carniato, F.; Bisio, C. *Proc. R. Soc. A* **2012**, *468*, 1904−1926.
(14) Maity, P.; Yamazoe, S.; Tsukuda, T. *ACS Catal.* **2013**, *3*, 182−185.
(15) Taketoshi, A.; Haruta, M. *Chem. Lett.* **2014**, *43*, 380−387.
(16) Perdew, J. P. In *Electronic Structure of Solids '91*; Ziesche, P., Eschrig, H., Eds.; Akademie Verlag: Berlin, 1991; p 11.
(17) Zhao, Y.; Pu, J.; Lynch, B. J.; Truhlar, D. G. *Phys. Chem. Chem. Phys.* **2004**, *6*, 673−676.
(18) Zheng, J.; Zhao, Y.; Truhlar, D. G. *J. Chem. Theory Comput.* **2007**, *3*, 569−582.
(19) Zhao, Y.; Truhlar, D. G. *J. Chem. Phys.* **2006**, *125*, 194101/1−194101/17.
(20) Peverati, R.; Truhlar, D. G. *J. Phys. Chem. Lett.* **2012**, *3*, 117−124.
(21) Peverati, R.; Truhlar, D. G. *Phys. Chem. Chem. Phys.* **2012**, *14*, 13171/1−13171/4.
(22) Andersson, Y.; Langreth, D. C.; Lundqvist, B. I. *Phys. Rev. Lett.* **1996**, *76*, 102−105.
(23) Yan, Z.; Perdew, J. P.; Kurth, S. *Phys. Rev. B* **2000**, *61*, 16430−16439.
(24) Furche, F. *Phys. Rev. B* **2001**, *64*, 195120/1−195120/8.
(25) Zhao, Y.; Lynch, B. J.; Truhlar, D. G. *J. Phys. Chem. A* **2004**, *108*, 4786−4791.
(26) Grimme, S. *J. Chem. Phys.* **2006**, *124*, 034108/1−034108/16.
(27) Vydrov, O. A.; Van Voorhis, T. *J. Chem. Phys.* **2009**, *130*, 104105/1−104105/7.
(28) Schimka, L.; Harl, J.; Stroppa, A.; Grüneis, A.; Marsman, M.; Mittendorfer, F.; Kresse, G. *Nat. Mater.* **2010**, *9*, 741−744.
(29) Göltl, F.; Grüneis, A.; Bučko, T.; Hafner, J. *J. Chem. Phys.* **2012**, *137*, 114111/1−114111/6.
(30) Karlický, F.; Lazar, P.; Dubecký, M.; Otyepka, M. *J. Chem. Theory Comput.* **2013**, *9*, 3670−3676.

(31) Perdew, J. P.; Burke, K.; Ernzerhof, M. *Phys. Rev. Lett.* **1996**, 77, 3865−3868.

(32) Bohm, D.; Pines, D. *Phys. Rev.* **1951**, 82, 625−634.

(33) Pines, D.; Bohm, D. *Phys. Rev.* **1952**, 85, 338−353.

(34) Bohm, D.; Pines, D. *Phys. Rev.* **1953**, 92, 609−625.

(35) Harl, J.; Schimka, L.; Kresse, G. *Phys. Rev. B* **2010**, 81, 115126/ 1−115126/18.

(36) Ren, A.; Rinke, P.; Joas, C.; Scheffler, M. *J. Mater. Sci.* **2012**, 47, 7447−7471.

(37) Eshuis, H.; Bates, J. E.; Furche, F. *Theor. Chem. Acc.* **2012**, 131, 1084/1−1084/18.

(38) Zhao, Y.; Truhlar, D. G. *Acc. Chem. Res.* **2008**, 41, 157−167.

(39) Zhao, Y.; Truhlar, D. G. *Chem. Phys. Lett.* **2011**, 502, 1−13.

(40) Peverati, R.; Truhlar, D. G. *Philos. Trans. R. Soc. A* **2014**, 372, 20120476/1−20120476/51.

(41) Karlický, F.; Otyepka, M. *J. Chem. Theory Comput.* **2011**, 7, 2876−2885.

(42) Filip, J.; Karlický, F.; Marusak, Z.; Lazar, P.; Černík, M.; Otyepka, M.; Zboril, R. *J. Phys. Chem. C* **2014**, 118, 13817−13825.

(43) Karlický, F.; Otyepka, M. *Int. J. Quantum Chem.* **2014**, 114, 987−992.

(44) Eder, M.; Terakura, K. *Phys. Rev. B* **2001**, 64, 115426/1− 115426/7.

(45) Lazar, P.; Otyepka, M. *J. Phys. Chem. C* **2012**, 116, 25470− 25477.

(46) Dunning, T. H. *J. Chem. Phys.* **1989**, 90, 1007−1023.

(47) Balabanov, N. B.; Peterson, K. A. *J. Chem. Phys.* **2005**, 123, 064107/1−064107/15.

(48) Seeger, R.; Pople, J. A. *J. Chem. Phys.* **1977**, 66, 3045−3050.

(49) Bauernschmitt, R.; Ahlrichs, R. *J. Chem. Phys.* **1996**, 104, 9047− 9052.

(50) (a) Becke, A. D. *Phys. Rev. A* **1988**, 38, 3098−3100. (b) Lee, C.; Yang, W.; Parr, R. G. *Phys. Rev. B* **1988**, 37, 785−789.

(51) Schultz, N. E.; Zhao, Y.; Truhlar, D. G. *J. Phys. Chem. A* **2005**, 109, 11127−11143.

(52) Dahlke, E. E.; Truhlar, D. G. *J. Phys. Chem. B* **2005**, 109, 15677−15683.

(53) Perdew, J.; Ruzsinszky, A.; Csonka, G. I.; Vydrov, O. A.; Scuseria, G. E. *Phys. Rev. Lett.* **2008**, 100, 136406/1−136406/4.

(54) Zhao, Y.; Truhlar, D. G. *J. Chem. Phys.* **2008**, 128, 184109/1− 184109/8.

(55) Peverati, R.; Zhao, Y.; Truhlar, D. G. *J. Phys. Chem. Lett.* **2011**, 2, 1991−1997.

(56) Peverati, R.; Truhlar, D. G. *J. Chem. Theory Comput.* **2012**, 8, 2310−2319.

(57) Perdew, J. P.; Ruzsinszky, A.; Csonka, G. I.; Constantin, L. A. *Phys. Rev. Lett.* **2009**, 103, 026403/1−026403/4 Erratum: **2011**, 106 179902(E) .

(58) Boese, A. D.; Handy, N. C. *J. Chem. Phys.* **2002**, 116, 9559− 9569.

(59) Stephens, P. J.; Devlin, F. J.; Chabalowski, C. F.; Frisch, M. J. *J. Phys. Chem.* **1994**, 98, 11623−11627.

(60) Hamprecht, F. A.; Cohen, A. J.; Tozer, D. J.; Handy, N. C. *J. Chem. Phys.* **1998**, 109, 6264−6271.

(61) Wilson, P. J.; Bradley, T. J.; Tozer, D. J. *J. Chem. Phys.* **2001**, 115, 9233−9242.

(62) Keal, T. W.; Tozer, D. J. *J. Chem. Phys.* **2005**, 123, 121103/1− 121103/4.

(63) Lynch, B. J.; Fast, P. L.; Harris, M.; Truhlar, D. G. *J. Phys. Chem. A* **2000**, 104, 4811−4815.

(64) Adamo, C.; Barone, V. *J. Chem. Phys.* **1999**, 110, 6158−6170.

(65) Peverati, R.; Truhlar, D. G. *J. Chem. Phys.* **2011**, 135, 191102/ 1−191102/4.

(66) Zhao, Y.; Schultz, N. E.; Truhlar, D. G. *J. Chem. Phys.* **2005**, 123, 161103/1−161103/4.

(67) Zhao, Y.; Schultz, N. E.; Truhlar, D. G. *J. Chem. Theory Comput.* **2006**, 2, 364−382.

(68) Zhao, Y.; Truhlar, D. G. *Theor. Chem. Acc.* **2008**, 120, 215−241.

(69) Zhao, Y.; Truhlar, D. G. *J. Phys. Chem. A* **2006**, 110, 13126− 13130.

(70) Zhao, Y.; Truhlar, D. G. *J. Chem. Theory Comput.* **2008**, 4, 1849−1868.

(71) Zhao, Y.; Truhlar, D. G. *J. Phys. Chem. A* **2005**, 109, 5656−5667.

(72) Chai, J. D.; Head-Gordon, M. *J. Chem. Phys.* **2008**, 128, 084106/ 1−084106/15.

(73) Peverati, R.; Truhlar, D. G. *J. Phys. Chem. Lett.* **2011**, 2, 2810− 2817.

(74) Krukau, A. V.; Vydrov, O. A.; Izmaylov, A. F.; Scuseria, G. E. *J. Chem. Phys.* **2006**, 125, 224106/1−224106/5.

(75) Peverati, R.; Truhlar, D. G. *Phys. Chem. Chem. Phys.* **2012**, 14, 16187−16191.

(76) Grimme, S.; Antony, J.; Ehrlich, S.; Krieg, H. *J. Chem. Phys.* **2010**, 132, 154104/1−154104/19.

(77) Grimme, S.; Ehrlich, S.; Goerigk, L. *J. Comput. Chem.* **2011**, 32, 1456−1465.

(78) Chai, J. D.; Head-Gordon, M. *Phys. Chem. Chem. Phys.* **2008**, 10, 6615−6620.

(79) Zhang, W.; Truhlar, D. G.; Tang, M. *J. Chem. Theory Comput.* **2013**, 9, 3965−3977.

(80) Pople, J. A.; Head-Gordon, M.; Raghavachari, K. *J. Chem. Phys.* **1987**, 87, 5968−5975.

(81) Douglas, M.; Kroll, N. M. *Ann. Phys.* **1974**, 82, 89−155.

(82) Hess, B. A. *Phys. Rev. A* **1985**, 32, 756−763.

(83) Hess, B. A. *Phys. Rev. A* **1986**, 33, 3742−3748.

(84) Jansen, G.; Hess, B. A. *Phys. Rev. A* **1989**, 39, 6016−6017.

(85) Martin, J. M. L. *ACS Symp. Ser.* **1998**, 677, 212−236.

(86) Truhlar, D. G. *Chem. Phys. Lett.* **1998**, 294, 45−48.

(87) Karton, A.; Martin, J. M. L. *Theor. Chem. Acc.* **2006**, 115, 330− 333.

(88) Halkier, A.; Helgaker, T.; Jørgensen, P.; Klopper, W.; Koch, H.; Jeppe, O.; Wilson, A. K. *Chem. Phys. Lett.* **1998**, 286, 243−252.

(89) Frisch, M. J.; Trucks, G. W.; Schlegel, H. B.; Scuseria, G. E.; Robb, M. A.; Cheeseman, J. R.; Scalmani, G.; Barone, V.; Mennucci, B.; Petersson, G. A. et al. *Gaussian 09*; Gaussian, Inc., Wallingford, CT, 2009.

(90) Werner, H.-J.; Knowles, P. J.; Manby, F. R.; Schütz, M.; Celani, P.; Knizia, G.; Korona, T.; Lindh, R.; Mitrushenkov, A.; Rauhut, G.; Adler, T. B.; Amos, R. D.; Bernhardsson, A.; Berning, A.; Cooper, D. L.; Deegan, M. J. O.; Dobbyn, A. J.; Eckert, F.; Goll, E.; Hampel, C.; Hesselmann, A.; Hetzer, G.; Hrenar, T.; Jansen, G.; Köppl, C.; Liu, Y.; Lloyd, A. W.; Mata, R. A.; May, A. J.; McNicholas, S. J.; Meyer, W.; Mura, M. E.; Nicklaß,A.; Palmieri, P.; Pflüger, K.; Pitzer, R. M.; Reiher, M.; Shiozaki, T.; Stoll, H.; Stone, A. J.; Tarroni, R.; Thorsteinsson, T.; Wang, M.; Wolf, A. *Molpro, version 2010.1*; University of Birmingham: Birmingham, U.K., 2010.

(91) Kresse, G.; Hafner, J. *Phys. Rev. B* **1993**, 47, 558−561. Kresse, G.; Hafner, J. *Phys. Rev. B* **1994**, 49, 14251−14269.

(92) Kresse, G.; Furthmuller, J. *Phys. Rev. B* **1996**, 54, 11169−11186.

(93) Blohl, P. E. *Phys. Rev. B* **1994**, 50, 17953−17979.

(94) Kresse, G.; Joubert, D. *Phys. Rev. B* **1999**, 59, 1758−1775.

(95) Ren, A.; Rinke, P.; Scheffler, M. *Phys. Rev. B* **2009**, 80, 045402/ 1−045402/8.

(96) Methfessel, M.; Paxton, A. T. *Phys. Rev. B* **1989**, 40, 3616−3621.

(97) Henkelman, G.; Uberuaga, B. P.; Jonsson, H. *J. Chem. Phys.* **2000**, 113, 9901−9904.

(98) Bitzek, E.; Koskinen, P.; Gahler, F.; Moseler, M.; Gumbsch, P. *Phys. Rev. Lett.* **2006**, 97, 107201/1−107201/4.

(99) Sheppard, D.; Terrell, R.; Henkelman, G. *J. Chem. Phys.* **2008**, 128, 134106/1−134106/10.

(100) Xu, X.; Zhang, W.; Tang, M.; Truhlar, D. G. to be published.

(101) Zhao, Y.; Ng, H. T.; Peverati, R.; Truhlar, D. G. *J. Chem. Theory Comput.* **2012**, 8, 2824−2834.

(102) Zhao, Y.; Truhlar, D. G. *J. Phys. Chem. A* **2005**, 109, 6624− 6627.

(103) Scuseria, G. E.; Henderson, T. M.; Sorensen, D. C. *J. Chem. Phys.* **2008**, 129, 231101/1−231101/4.

(104) Zheng, J.; Zhao, Y.; Truhlar, D. G. *J. Chem. Theory Comput.* **2009**, *5*, 808−821.

(105) Lynch, B. J.; Zhao, Y.; Truhlar, D. G. *J. Phys. Chem. A* **2005**, *109*, 1643−1649.

(106) Zhao, Y.; Lynch, B. J.; Truhlar, D. G. *Phys. Chem. Chem. Phys.* **2005**, *7*, 43−52.